Environmental Chemistry Letters (2021) 19:3505–3510
https://doi.org/10.1007/s10311-021-01221-y

ORIGINAL PAPER

Efficient honeycomb–shaped biochar anodes for lithium-ion batteries from *Eichhornia crassipes* biomass

Xueli Chen[1] · Feng Li[1] · Shibiao Su[2] · Hongyu Chen[1] · Jiahui Zhang[2] · Dandan Cai[2]

Received: 20 November 2020 / Accepted: 10 March 2021 / Published online: 22 April 2021

Abstract

Converting waste biomass into biochar is a means for solving both environmental pollution and energy shortage. Here we transformed *Eichhornia crassipes*, a harmful floating plant, into a honeycomb-shaped and heteroatoms-rich biochar by KOH activation during carbonization, and we tested this biochar as anode for lithium-ion batteries. Results show that the biochar has a high surface area of 278.56 $m^2 \cdot g^{-1}$, a honeycomb-like porous structure, and is rich in heteroatoms, e.g., 3.42% N, 20.82% O, and 0.83% S. Biochar anodes displayed a higher initial reversible specific capacity of 697 $mAh \cdot g^{-1}$ at 50 $mA \cdot g^{-1}$, a higher rate capability of 229.7 $mAh \cdot g^{-1}$ at 3000 $mA \cdot g^{-1}$, and a better cyclic stability than commercial graphite. The enhanced electrochemical performance could be attributed to the interconnected porous structure that promotes Li^+ transfer and electrolyte infiltration, and to the presence of heteroatoms. This approach can be easily industrialized as a substitute of graphite.

Keywords Trash reclamation · *Eichhornia crassipes* · Biochar anode · Honeycomb-shaped · Heteroatoms-rich · Lithium-ion batteries

Introduction

With the growth of the growing population and economy, energy and environmental crises have become the focus of attention. Rechargeable lithium-ion batteries have received increasing attention in energy storage devices due to their high energy density, long cycling life, eco-friendliness, and safety (Wu et al. 2020). Owing to its long-term cycling stability and low working voltage (*versus* Li/Li^+), graphite is widely commercial anode material for lithium-ion batteries (Fang et al. 2019). But the low theoretical specific capacity (372 $mAh \cdot g^{-1}$) and poor rate performance greatly limit its application in lithium-ion batteries (Yang et al. 2020). Compared to graphene, porous carbon materials have attracted increasing attention in lithium-ion batteries because they show high specific capacity and good rate performance, because porous carbon can offer a large electrode/electrolyte interface for the charge transfer and provides shorter diffusion pathways for Li^+ and electrolyte (Yu et al. 2016). On the other hand, the heteroatoms-rich (N, P, S) of porous carbon has been proven to improve the electrochemical performance because heteroatoms have a different electronegativity compared with C atoms, and then as it can provide more active sites and enhance carbon materials reactivity (Wang et al. 2013). As we all know, biomass, as environmental-friendly and low-cost sustainable resource, has already been proved attractive raw materials for fabricating heteroatoms-rich porous carbon materials.

Biomass waste is generated in ecological circulation and causes severe resource waste and environmental pollutions when inappropriately managed and treated; therefore, transforming biomass waste into useful products based on the idea of "trash to treasure" is urgently required (Wang et al. 2020; Tuck et al. 2012). *Eichhornia crassipes* (*E. crassipes*) is an exotic plant ubiquitously found in various water environment, and its high rates of regeneration and uncontrolled growth have caused safety issues to sailing industry and ecological concerns to local fisheries (Mahamadi et al. 2014). *E. crassipes*, as a renewable and sustainable source, has transformed into biofuels, bioethanol, and biochar (Akhil et al. 2021). In particular,

✉ Feng Li
hjlifeng@scut.edu.cn

✉ Dandan Cai
caidandan86@mailbox.gxnu.edu.cn

[1] School of Civil Engineering & Transportation, South China University of Technology, Guangzhou 510641, China

[2] Guangxi Key Laboratory of Low Carbon Energy Materials, Guangxi Normal University, Guilin 541004, China

E. crassipes-derived biochar has been successfully applied in many fields, such as the remediation of pollutions in soil and wastewater, due to its excellent physical and chemical properties (Chen et al. 2018; 2019). Recently, increasing number of researchers focus on biochar-based materials for energy storage and conversion given its large surface area, high porosity, inherent heteroatoms-rich, and amorphous carbon matrix (Liu et al. 2019; Tan et al. 2012). However, application of the *E. crassipes*-derived biochar for energy storage has been rarely reported.

Herein, a honeycomb-shaped and heteroatoms-rich biochar is prepared by carbonizing waste *E. crassipes*, which is applied as anode for lithium-ion batteries. Notably, the abundant porosity and high surface area of biochar could facilitate electrons and Li^+ diffusion, and the heteroatoms-rich (N, O, S) of biochar can tailor the electronic structure. The biochar shows good electrochemical performance, including high specific capacity, cycle stability, and rate performance. The present work provides a substitute for graphite production and for solving both environmental pollution and energy storage issues; moreover, this kind of carbon materials can be easily industrialized.

Results and discussion

Structure characterization

E. crassipes were chosen as the promising candidates to fabricate the porous biochar because not only they possess porous cell wall-like structure (Fig. S1), but also they are inherent heteroatoms-rich. The detailed synthesis procedures are illustrated (Fig. 1a). The biochar revealed a hierarchical porous structure with abundant channels and smooth surface, and these pores and channels were interconnected similar to a honeycomb structure (Fig. 1b, c). High-resolution transmission electron microscopy images confirm biochar shows porous carbon with a disordering microstructure (Fig. S2). Furthermore, signals of C (74.93%), N (3.42%), O (20.82%), and S (0.83%) elements were recorded

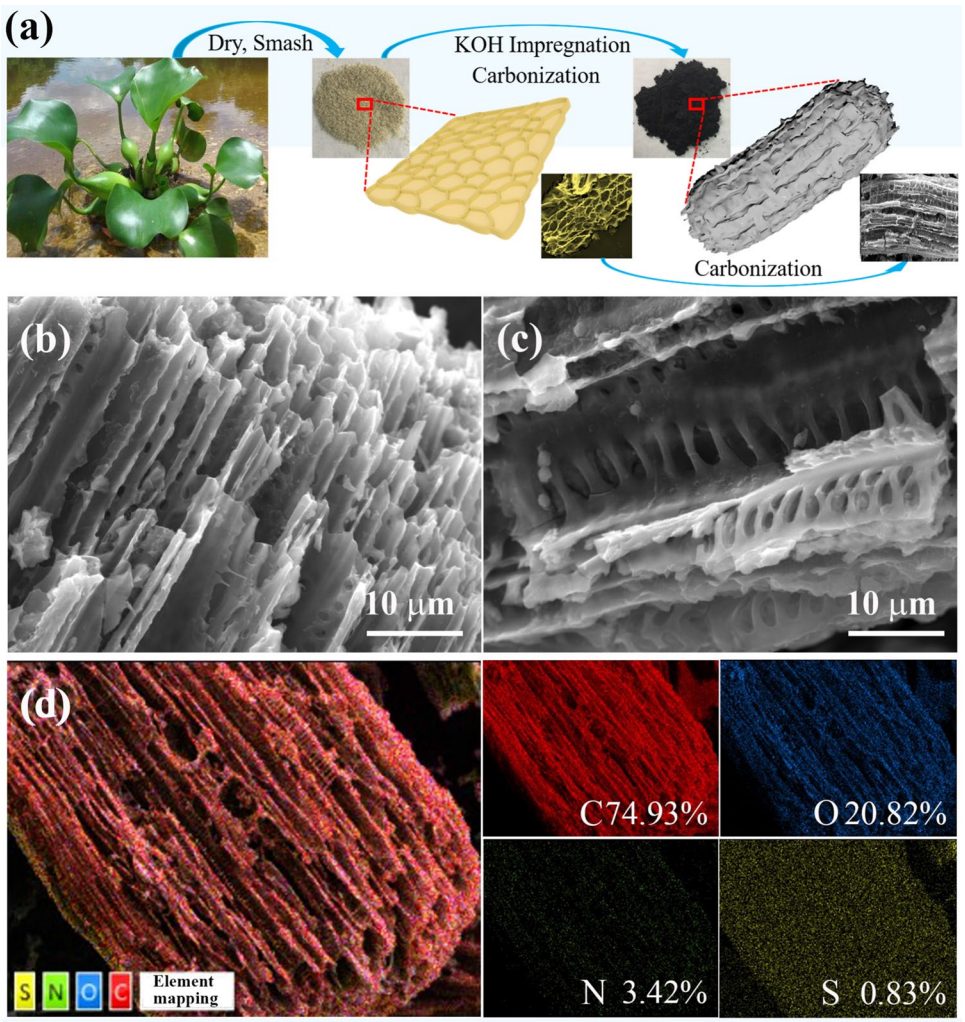

Fig. 1 Synthesis process of *E. crassipes*-derived biochar (**a**); scanning electron microscopy images (**b**, **c**); and elemental mapping of C, N, O, and S (**d**)

in elemental mapping images of biochar (Fig. 1d). The broad diffraction peak centered at $2\theta = 24.16°$, which is assigned to disordered carbon (002) plane (Wang et al. 2013), and the weak diffraction peaks centered at $2\theta = 42.37°$, corresponding to the crystalline carbon structure (100) plane (JCPDS #41–1487, Fig. 2a). Moreover, the calculated average interlayer spacing (d_{002}) for biochar is 0.367 nm according to Bragg's equation ($d = n\lambda/2\sin\theta$), which is larger than that of graphite (0.334 nm), and indicates that the heteroatoms are located into carbon matrix.

Three characteristic Raman peaks were observed at 1359 cm^{-1} (D band), 1590 cm^{-1} (G band), and 2852 cm^{-1} (D* band) (Fig. 2b). The I_D/I_G ratio is 0.846, which demonstrates that biochar possesses defect structures and graphite layers (Li et al. 2013). Several functional groups characteristic peaks were observed in Fourier transform infrared spectroscopy spectra (Fig. 2d), including 3438 cm^{-1} (O – H groups from surface-bound water molecules) (Yu et al. 2016), 2350 cm^{-1} (O – C = O vibrations), 1709 cm^{-1} (C = O/N), 1612 cm^{-1} (C = C in aromatic ring), 1428 cm^{-1} (C – N stretching vibrations), 1237 cm^{-1} (C – N/O), 1027 cm^{-1} (C – S), and 673 cm^{-1} (O – H) (Li et al. 2020). Moreover, the absorption–desorption curve of biochar showed a type-I isotherm featured with H_2 hysteresis, revealing the existence of microporous property. The Brunauer–Emmett–Teller surface area can be up to 278.56 $m^2 \cdot g^{-1}$ (Figs. 2c, S3). The pore size distributions of biochar were estimated using nonlocal density functional theory (Fig. S5), indicating that biochar possesses the micropores (8–12 Å).

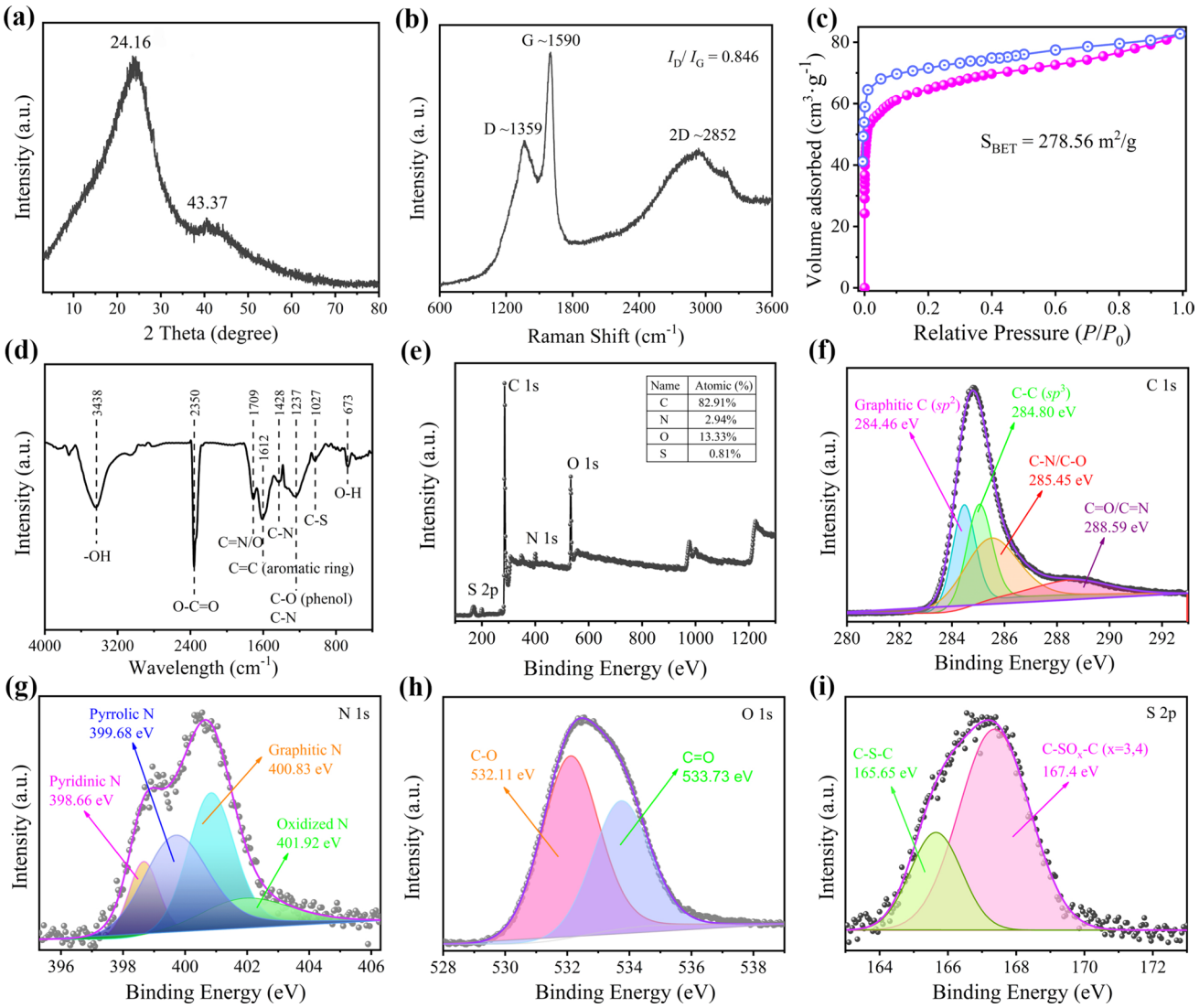

Fig. 2 Characterization of biochar. X-ray diffractometry pattern (**a**); Raman spectra (**b**); nitrogen adsorption/desorption isotherm, Brunauer–Emmett–Teller surface area linear equation: $V/V_m = [P/(P_0 - P)]/\{(1/C) + [(C-1)/C](P/P_0)\}$ (**c**); Fourier transform infrared spectrum (**d**); X-ray photoelectron spectroscopy spectrum of all survey (**e**); C 1 s (**f**); N 1 s (**g**); O 1 s (**h**); S 2p (**i**)

The chemical bonding environment of biochar was characterized by the X-ray photoelectron spectroscopy (Fig. 2e). It is observed that the biochar is made up of C (82.91 at%), N (2.94 at%), O (13.33 at%), and S (0.81 at%), respectively, which are almost consistent with the energy-dispersive X-ray spectroscopy results. The C 1 s spectra (Fig. 2f) exhibited four bands, related to the graphitic C (sp^2, 284.6 eV), C – C (sp^3, 285.0 eV), C – N/O (285.6 eV), and C = N/O (288.3 eV) (Singh et al. 2014). The peak of N 1 s was observed at 400 eV (Fig. 2g), which was deconvoluted into four peaks at 398.8 eV (pyridinic – N), 400.5 eV (pyrrolic – N), 401.2 eV (graphitic – N), and 404.5 eV (oxidized – N). The O 1 s spectra can be deconvoluted into two peaks at 531.8 and 533.4 eV (Fig. 2h), assigned to the C – O and C = O groups (Wang et al. 2013). Moreover, the S 2p spectra were deconvoluted into two peaks at 165.65 and 167.4 eV (Fig. 2i), assigned to the C–S–C bond (thiophene-S structure) and the oxidized sulfur groups (C–$SO_{3/4}$–C) (Huo et al. 2018).

Electrochemical performance

The electrochemical performance of biochar anode for lithium-ion batteries was investigated in a coin cell countered with a lithium foil counter electrode (Cai et al. 2016). Cyclic voltammograms of the anode were conducted to investigate the kinetic process in the initial three cycles in the potential range of 0.01–3.0 V (*versus* Li/Li^+) at a scanning rate of 0.1 $mV{\cdot}s^{-1}$ (Fig. 3a), consistent with those of previously reported carbon-based anode materials (Wu et al. 2020). In the first cycle, the reduction peak located at 1.16~0.36 V is due to the formation of a solid-electrolyte interphase on the surface of the biochar. The cyclic voltammograms curves almost overlapped in the following two cycles, indicative of the formation of a stable solid-electrolyte interphase layer (Fang et al. 2019).

The galvanostatic discharge/charge curves for three cycles of anode are at a current density of 50 $mA{\cdot}g^{-1}$ in the voltage range of 0.01~3.0 V (*versus* Li/Li^+) (Fig. 3b). The

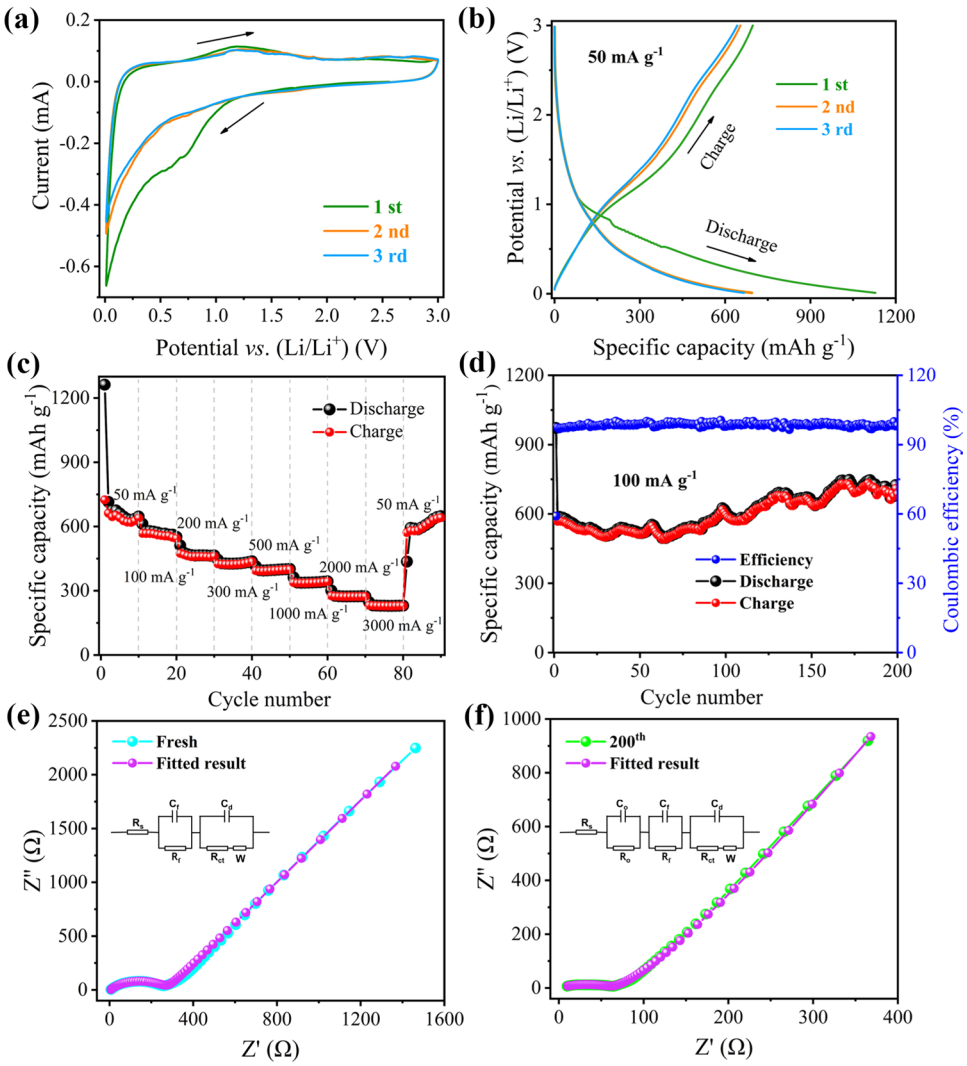

Fig. 3 Cyclic voltammograms curves, *versus* Li/Li^+, at a scanning rate of 0.2 $mV{\cdot}s^{-1}$ (**a**); first-three galvanostatic discharge/charge voltage *versus* specific capacity curves (**b**); rate capabilities at various current densities (**c**); cycle performance and Coulombic efficiency (**d**); solid-electrolyte interphase spectra of fresh anode (**e**); after 200 charge/discharge cycles (**f**)

shape of the discharge/charge profiles matches well with the cyclic voltammograms curves. The initial reversible specific capacity of anode is approximately 697 ± 4.3 mAh·g^{-1} at 50 mA·g^{-1}. The galvanostatic discharge/charge curve of biochar matched well with the representative plot of hard carbon anode (Yu et al. 2016). The initial high discharge capacity (1131 mAh·g^{-1}) can be assigned to the presence of abundant channels and pores in its structure. The initial capacity loss was possibly attributed to the formation of the solid-electrolyte interphase layer in the irreversible processes (Wei et al. 2016). Moreover, the solid-electrolyte interphase layer and the inevitable decomposition of electrolyte as well as the insertion of Li^+ of biochar after the first cycle irreversible reactions resulted in a long slope of the initial discharge curve (Su et al. 2011). The discharge/charge capacities were approximately 697/652 and 666/640 mAh·g^{-1} for the second and third cycles. Meanwhile, the similar reversible specific capacities for the second and third cycles suggest a good reversibility of anode for lithium-ion batteries. Moreover, the specific capacity of the voltage region below 1.0 V (*versus* Li/Li^+) was mainly due to the Li^+ intercalation into the porous structure of biochar.

Rate capability was performed with increasing current densities from 50 to 3000 mA·g^{-1} (Fig. 3c). The specific capacities of 624.8 ± 53.2, 559.4 ± 14.7, 462.5 ± 4.5, 426.3 ± 3.7, 395.2 ± 3.3, 338.2 ± 2.9, 273.5 ± 3.4, and 229.7 ± 0.9 mAh·g^{-1} were obtained at various current densities of 50, 100, 200, 300, 500, 1000, 2000, and 3000 mA·g^{-1}, respectively. The significant rate capability originated from the interconnected porous structure and graphene layers of biochar (Liu et al. 2019). Noticeably, when the current density returned to 50 mA·g^{-1} after cycling at different current densities, the reversible capacity of 649.8 ± 1.8 mAh·g^{-1} was well recovered, suggesting that the anode possesses a good electrochemical stability.

The cycle performance and Coulombic efficiency were investigated at a current density of 100 mA·g^{-1} (Fig. 3d). In the second reversible specific capacity of 597.9 mAh·g^{-1}, it was much higher than those of the conventional graphite materials (372 mAh·g^{-1}). Subsequently, it remained stable in capacity earlier at the 60th cycle, and then the slight increase in capacity from 60 to 170 cycles was due to the possible activation process of anode and the continuously trapped Li^+ (Su et al. 2011). The anode can sustain high capacity of 720 ± 30.2 mAh·g^{-1} at 100 mA·g^{-1} even after 200 cycles. The electrochemical performance of biochar in our work has been compared with other biomass-derived carbon anodes for lithium-ion batteries (Table S2). The high oxygen content could cause in the irreversible reaction to produce Li_2O (Dong et al. 2018). Thus, the reversible specific capacity decreases with oxygen content increased, resulting in the low initial Coulomb efficiency (Cai et al. 2018; Matsuo et al. 2018).

To understand the electrochemical characteristics of anode, the electrochemical impedance spectroscopy data for the anode of fresh and after 1st, 200th cycles were measured and corresponding Nyquist plots were obtained (Figs. 3e-3f, S6). The electrochemical impedance spectroscopy spectra were fitted by *ZSimpWin* software based on the electrical equivalent circuit (Table S1) (Han et al. 2011). The Nyquist plots include a semicircle at the high-frequency region and a straight line over the low-frequency region, where R_s is the solution resistance, R_{ct} is the charge/transfer resistance, R_o is the interface resistance, and R_f is the solid-electrolyte interphase resistance (Yu et al. 2016). A smaller semicircle diameter and a larger slope of the straight line after 1st, 200th cycles indicate the favorable ionic diffusion and charge transport in anode. The values of R_o/R_{ct} decrease and R_f increase for anode after first cycle compared with those of the fresh anode, which might be attributed to the inevitable decomposition of electrolyte, the insertion of Li^+ of biochar, and the formation of solid-electrolyte interphase (Han et al. 2011). Moreover, the structure after 200th cycles was almost unchanged compared with the fresh anode (Fig. S7). These results suggesting the anode resistance is stabilized, and the biochar can stabilize the solid-electrolyte interphase layer. The prominent electrochemical performance of anode could be ascribed to the following reasons: (1) *E. crassipes*-derived biochar not only offers large electrode/electrolyte contact area but also sufficient space for Li^+; (2) interconnected structures shortened the Li^+ diffusion pathway; (3) graphene and heteroatom-rich boosted the electronic conductivity and electrochemical stability.

Conclusion

Hierarchically porous heteroatoms-rich biochar was successfully prepared from *E. crassipes* and used as anodes for lithium-ion batteries. The biochar exhibits a good rate capacity of 229.7 ± 0.9 mAh·g^{-1} at 3000 mA·g^{-1} and high initial reversible specific capacity of 697 ± 4.3 mAh·g^{-1} at 50 mA·g^{-1}, and the remaining capacity was 720 ± 30.2 mAh·g^{-1} after 200 cycles. The superior electrochemical performance of biochar could be ascribed to hierarchically porous structure and high surface area and inherent heteroatom rich. This approach can easily realize industrial production, and it will have a promising application in energy storage and environmental issues. Moreover, porous carbon is expected to be applied to other fields such as supercapacitors, catalysis, adsorption, and pollutants purification.

Supplementary Information The online version contains supplementary material available at https://doi.org/10.1007/s10311-021-01221-y.

Acknowledgements This work was supported by National Key Research and Development Program of China (2016YFC0402600), National Natural Science Foundation of China (No.41001341, 21661008), Water Conservancy Science and Technology Innovation Project of Guangdong Province (2017-21), and Fundamental Research Funds for the Central Universities (2019-17).

References

Akhil D, Lakshmi D et al (2021) Production, characterization, activation and environmental applications of engineered biochar: a review. Environ Chem Lett. https://doi.org/10.1007/s10311-020-01167-7

Cai D, Li D et al (2016) Interconnected α-Fe_2O_3 nanosheet arrays as high-performance anode materials for lithium-ion batteries. Electrochim Acta 192:407–413. https://doi.org/10.1016/j.electacta.2016.02.010

Cai D, Wang C et al (2018) Facile synthesis of N and S co-doped graphene sheets as anode materials for high-performance lithium-ion batteries. J Alloy Compd 731:235–242. https://doi.org/10.1016/j.jallcom.2017.10.043

Chen XL, Li F et al (2019) Nanoscale zero-valent iron and chitosan functionalized *Eichhornia crassipes* Biochar for Efficient Hexavalent Chromium Removal. Int J Environ Res Public Health 16(17):3046. https://doi.org/10.3390/ijerph16173046

Chen L, Li F et al (2018) High cadmium adsorption on nanoscale zero-valent iron coated *Eichhornia crassipes* biochar. Environ Chem Lett 17(1):589–594. https://doi.org/10.1007/s10311-018-0811-y

Dong Q, Hong B et al (2018) Electron-rich functional doping carbon host as dendrite-free lithium metal anode. Electrochim Acta 284:376–381. https://doi.org/10.1016/j.electacta.2018.07.161

Fang R, Chen K et al (2019) The regulating role of Carbon nanotubes and graphene in lithium-ion and lithium-sulfur batteries. Adv Mater 31(9):1800863. https://doi.org/10.1002/adma.201800863

Han FD, Bai YJ et al (2011) Template-free synthesis of interconnected hollow carbon nanospheres for high-performance anode material in lithium-ion batteries. Adv Energy Mater 1(5):798–801. https://doi.org/10.1002/aenm.201100340

Huo S, Liu MQ et al (2018) Methanesulfonic acid-assisted synthesis of N/S co-doped hierarchically porous carbon for high performance supercapacitors. J Power Sour 387:81–90. https://doi.org/10.1016/j.jpowsour.2018.03.061

Li X, Xu Y et al (2020) Increasing the heteroatoms doping percentages of graphene by porous engineering for enhanced electrocatalytic activities. J Colloid Interface Sci 577:101–108. https://doi.org/10.1016/j.jcis.2020.05.089

Li Z, Xu Z et al (2013) Mesoporous nitrogen-rich carbons derived from protein for ultra-high- capacity battery anodes and supercapacitors. Energy Environ Sci 6(3):871. https://doi.org/10.1039/c2ee23599d

Liu WJ, Jiang H, Yu HQ (2019) Emerging applications of biochar-based materials for energy storage and conversion. Energy Environ Sci 12:1751–1779. https://doi.org/10.1039/c9ee00206e

Mahamadi C, Mawere E (2014) High adsorption of dyes by water hyacinth fixed on alginate. Environ Chem Lett 12:313–320. https://doi.org/10.1007/s10311-013-0445-z

Matsuo Y, Taninaka J et al (2018) Effect of oxygen contents in graphene like graphite anodes on their capacity for lithium-ion battery. J Power Sour 396:134–140. https://doi.org/10.1016/j.jpowsour.2018.06.022

Singh B, Fang Y, Cowie BCC, Thomsen L (2014) NEXAFS and XPS characterization of carbon functional groups of fresh and aged biochars. Org Geochem 77:1–10. https://doi.org/10.1016/j.orggeochem.2014.09.006

Su F, Poh CK et al (2011) Nitrogen-containing microporous carbon nanospheres with improved capacitive properties. Energy Environ Sci 4(3):717–724. https://doi.org/10.1039/c0ee00277a

Tan CW, Tan KH et al (2012) Energy and environmental applications of carbon nanotubes. Environ Chem Lett 10:265–273. https://doi.org/10.1007/s10311-012-0356-4

Tuck CO, Pérea E et al (2012) Valorization of biomass: deriving more value from waste. Sci 337:695–699. https://doi.org/10.1126/science.1218930

Wang D, Lee SH, Kim J, Park CB (2020) "Waste to Wealth": lignin as a renewable building block for energy harvesting/storage and environmental remediation. Chemsuschem 13(11):2807–2827. https://doi.org/10.1002/cssc.202000394

Wang L, Schnepp Z, Titirici MM (2013) Rice husk-derived carbon anodes for lithium-ion batteries. J Mater Chem A 1(17):5269–5273. https://doi.org/10.1039/c3ta10650k

Wei Y, Tao Y et al (2016) Unique electrochemical behavior of heterocyclic selenium–sulfur cathode materials in ether-based electrolytes for rechargeable lithium batteries. Energy Storage Mater 5:171–179. https://doi.org/10.1016/j.ensm.2016.07.005

Wu F, Maier J, Yu Y (2020) Guidelines and trends for next-generation rechargeable lithium and lithium-ion batteries. Chem Soc Rev 49(5):1569–1614. https://doi.org/10.1039/c7cs00863e

Yang C, Zhang X et al (2020) Holey graphite: A promising anode material with ultrahigh storage for lithium-ion battery. Electrochim Acta 346:136244. https://doi.org/10.1016/j.electacta.2020.136244

Yu W, Wang H et al (2016) N, O-codoped hierarchical porous carbons derived from algae for high-capacity supercapacitors and battery anodes. J Mater Chem A 4(16):5973–5983. https://doi.org/10.1039/c6ta01821a